Development/Plasticity/Repair

Katanin p60-like1 Promotes Microtubule Growth and Terminal Dendrite Stability in the Larval Class IV Sensory Neurons of *Drosophila*

Andrea Stewart,[1] Asako Tsubouchi,[2] Melissa M. Rolls,[3] W. Daniel Tracey,[2] and Nina Tang Sherwood[4]

[1]Department of Biology, Duke University, Durham, North Carolina 27708, [2]Departments of Anesthesiology, Cell Biology and Neurobiology, Duke University, Durham, North Carolina 27710, [3]Department of Biochemistry and Molecular Biology, The Pennsylvania State University, University Park, Pennsylvania 16802, and [4]Departments of Biology and Molecular Genetics and Microbiology, Duke University, Durham, North Carolina 27708

Dendrite shape is considered a defining component of neuronal function. Yet, the mechanisms specifying diverse dendritic morphologies, and the extent to which their function depends on these morphologies, remain unclear. Here, we demonstrate a requirement for the microtubule-severing protein katanin p60-like 1 (Kat-60L1) in regulating the elaborate dendrite morphology and nocifensive functions of *Drosophila* larval class IV dendritic arborization neurons. *Kat-60L1* mutants exhibit diminished responsiveness to noxious mechanical and thermal stimuli. Class IV dendrite branch number and length are also reduced, supporting a correspondence between neuronal function and the full extent of the dendritic arbor. These arborization defects occur particularly in late larval development, and live imaging reveals that Kat-60L1 is required for dynamic, filopodia-like nascent branches to stabilize during this stage. Mutant dendrites exhibit fewer EB1-GFP-labeled microtubules, suggesting that Kat-60L1 increases polymerizing microtubules to establish terminal branch stability and full arbor complexity. Although loss of the related microtubule-severing protein Spastin also reduces the class IV dendrite arbor, microtubule polymerization within dendrites is unaffected. Conversely, Spastin overexpression destroys stable microtubules within these neurons, while Kat-60L1 has no effect. Kat-60L1 thus sculpts the class IV dendritic arbor through microtubule regulatory mechanisms distinct from Spastin. Our data support differential roles of microtubule-severing proteins in regulating neuronal morphology and function, and provide evidence that dendritic arbor development is the product of multiple pathways functioning at distinct developmental stages.

Introduction

The remarkable diversity of neuronal dendrite morphology plays a central role in the specialized functions of neurons. Identification of the mechanisms conferring these varied morphologies, and the ways in which neurons' distinctive functions rely on them, is thus essential for understanding the nervous system. Both neuronal morphology and function depend on the microtubule cytoskeleton, in fundamental events including process outgrowth and stabilization, synapse formation, and vesicle transport. Consequently, microtubule maintenance, assembly, and disassembly are tightly regulated by numerous proteins. Among these, the microtubule-severing proteins use ATP hydrolysis to break microtubule polymers along their lengths or promote end depolymerization (Roll-Mecak and McNally, 2010; Sharp and Ross, 2012). At least three severing proteins, Katanin-60 (Kat60), Spastin, and Katanin p60-like1 (Kat-60L1), are expressed in the *Drosophila* nervous system. Studies of Kat60 and Spastin indicate that each assembles into hexameric rings to disrupt tubulin–tubulin contacts along microtubules, thereby breaking polymers into smaller pieces (McNally and Vale, 1993; Roll-Mecak and Vale, 2008). Severed pieces can be further disassembled, as observed *in vitro* (McNally and Vale, 1993; Zhang et al., 2007; Yu et al., 2008). However, severed polymers can also provide a source of more easily transported or nucleating pieces, thus promoting additional microtubule formation (Roll-Mecak and McNally, 2010).

The *Drosophila* dendritic arborization (da) neurons, a subset of the multidendritic (md) sensory neurons, innervate the overlying larval epidermis in a stereotyped pattern, providing nearly complete coverage. These neurons provide a valuable system for studying the correlation between dendritic form and function. Four classes of da neurons are distinguished according to their

Received Feb. 15, 2012; revised June 17, 2012; accepted July 5, 2012.

Author contributions: A.S., M.M.R., W.D.T., and N.T.S. designed research; A.S. and A.T. performed research; A.S., A.T., M.M.R., and W.D.T. contributed unpublished reagents/analytic tools; A.S. and N.T.S. analyzed data; A.S. and N.T.S. wrote the paper.

This work was supported by the National Institute of Neurological Disorders and Stroke (R01NS63896) (N.T.S.), the Spastic Paraplegia Foundation (N.T.S.), the Duke University Institute for Genome Sciences and Policy (N.T.S.), a National Science Foundation Graduate Research Fellowship (DGE-1106401) (A.S.), grants from the National Institutes of Health (R01GM086458 and R01NS054899) (W.D.T.), and National Institutes of Health Grant R01 GM085115 (M.M.R.). M.M.R. is a Pew Scholar in the Biomedical Sciences. We thank the reviewers of this manuscript for invaluable and insightful critiques. We thank Fang Du, Melissa Long, Floyd Mattie, Lixian Zhong, and Richard Hwang for excellent technical advice and assistance, as well as Margaret Naunheim for her work on the *kat-60L1* excision screen and Leah Croll for help with data analysis. Many thanks to David Sherwood, Kai Zinn, David Sharp, and members of the Sherwood laboratory for critical discussions, and to Doug Marchuk, Vann Bennett, and the Department of Molecular Genetics and Microbiology for their generous support. We are grateful to the Bloomington and Vienna stock centers for providing fly lines and to the Developmental Studies Hybridoma Bank for monoclonal antibodies.

The authors declare no competing financial interests.

Correspondence should be addressed to Nina Tang Sherwood at the above address. E-mail: ntangs@duke.edu.

DOI:10.1523/JNEUROSCI.0729-12.2012

 0270-6474/12/3211631-12$15.00/0

dendritic branching patterns and complexity, ranging from the class I neurons with simply constructed dendritic arbors, to the class IV neurons, which exhibit the most highly branched dendritic trees (Grueber et al., 2002). Activation of the complex class IV arbors is sufficient to mediate larval mechanical and thermal nociception (Hwang et al., 2007; Zhong et al., 2012).

A role for microtubule severing in the regulation of class IV da neuron dendrites is supported by studies demonstrating that *spastin* mutants, whether loss or gain of function, result in dendritic arbors of reduced complexity (Jinushi-Nakao et al., 2007; Ye et al., 2011). In addition, Kat-60L1 induces microtubule destruction during dendrite pruning of these neurons at metamorphosis (Lee et al., 2009). *In situ* data indicates that *kat-60L1* is also expressed in the embryonic nervous system, however, suggesting an important role even before metamorphosis (Tomancak et al., 2002).

In this study, we show a dendrite-specific, novel role for Kat-60L1 in the establishment of the class IV arbor during larval development. Using a combination of genetic, behavioral, and live imaging techniques, we reveal that *Drosophila* Kat-60L1 is required for the full extent of dendrite branching and elongation. Kat-60L1 increases the number of growing microtubules and the stability of terminal branches during late larval development. We also demonstrate a requirement for Kat-60L1 in the class IV-mediated larval nocifensive response, correlating defects in dendritic morphology to neuronal function. This correlation is also seen in *spastin* mutants; however, Spastin is not required for microtubule polymerization in dendrites and its loss affects neuronal function more broadly in the cell. Based on our data, we propose that Kat-60L1 plays a unique role in regulating microtubules to promote terminal arborization and function of class IV sensory neuron dendrites.

Materials and Methods

Drosophila *stocks and crosses.* The genetic deletion *Df(3R)kat-60L1^{BE6}* was created by imprecise excision of the neighboring enhancer-promoter (EP) insertion, *EY21697*, in the gene *CG2051*. Approximately 350 potential deletion lines were screened by PCR to uncover one deletion in *kat-60L1*, denoted *BE6*. A combination of primer walking and sequencing was used to delineate the breakpoints of *Df(3R)kat-60L1^{BE6}* to a 498 bp region, 3R:1609500-1609997, in the second intron of *kat-60L1*, and 3R: 1,614,857, where part of the EP remains in the genomic DNA of *CG2051*.

For *kat-60L1* loss-of-function analysis, we crossed *ppk1.9-GAL4, UAS-mCD8::GFP; kat-60L1^{BE6}/TM6b* to *kat-60L1$^{PBac\ c01236}$/TM6b*.

We used Vienna *Drosophila* RNAi Center (VDRC) *kat-60L1* RNAi lines 31599, 31598, and 108168, and VDRC *spastin* RNAi line 108739. For *kat-60L1* RNAi experiments, we crossed *ppk1.9-GAL4, UAS-mCD8::GFP* to a double RNAi stock, *kat-60L1$^{31599\ RNAi}$; kat-60L1$^{31598\ RNAi}$* or to *kat-60L1$^{108168\ RNAi}$*.

For rescue experiments, we crossed *ppk1.9-GAL4, UAS-mCD8::GFP; Df(3R)kat-60L1^{BE6}/TM6b* to *kat-60L1$^{PBac\ c01236}$*, *UAS-Venus-kat-60L1^{14}/TM6b* to obtain genetic rescue animals of the genotype *ppk1.9-GAL4, UAS-mCD8::GFP/+; Df(3R)kat-60L1^{BE6}/kat-60L1$^{PBac\ c01236}$*, *UAS-Venus-kat-60L1^{14}*.

For live EB1-GFP analysis, we crossed *477-GAL4, UAS-EB1-GFP/CyO; kat-60L1$^{PBac\ c01236}$/TM6b* to *Df(3R)kat-60L1^{BE6}/TM3 SerAct5c::GFP* to obtain larvae of the genotype *477-GAL4, UAS-EB1-GFP; kat-60L1$^{PBac\ c01236}$/ Df(3R)kat-60L1^{BE6}*. Control larvae were obtained from crosses of *477-GAL4, UAS-EB1-GFP/CyO* to *WCS*.

Drosophila stocks were provided by the Bloomington Stock Center (Bloomington, IN) and the VDRC (Vienna, Austria).

Reverse transcription PCR for developmental analysis of kat-60L1 isoforms. Primers were designed to amplify cDNA of both the *kat-60L1* short and long isoforms. The forward *kat-60L1-short* primer in exon 1 was AACGACTGGTGGAGCAAAAT. The forward *kat-60L1-long* primer in exon 1 was CGGCACACTCCATACCACT. Each was used with the shared reverse primer in the second exon: GCATTAGAGCCCAGGTTG. The short isoform primers amplify a predicted cDNA-specific 344 bp product and the long isoform primers amplify a predicted cDNA-specific 245 bp product. RNA was isolated by Trizol extraction from the following tissues: stage 11–17 embryos, third-instar larval brains, adult heads, adult testes, and adult ovaries; cDNA was generated using the Bioline cDNA kit (Bioline USA).

Reverse transcription PCR to characterize kat-60L1 *loss-of-function alleles and RNAi.* A forward primer specific to *kat-60L1* cDNA, spanning exon 3 and 4, excluding intronic sequence (Fig. 1*A*), GACAATACTCCAGGAAGCAGT, and a reverse primer in exon 5, ACGTTGCTTATGTCCGATCC, were used for all reverse transcription PCR (RT-PCR) experiments to characterize expression levels of *kat-60L1* loss-of-function mutant and RNAi backgrounds. RT-PCR was performed on samples of adult heads from *WCS* controls and *kat-60L1*-mutant animals and from larval brains of control and animals with either *kat-60L1* or *spastin* RNAi driven by the ubiquitous driver, *e22c-GAL4, sqh-GAL4*, and *UAS-Dicer2*. RNA was isolated and cDNA was generated as above.

Behavioral analysis. To perform the nociception assays, ~6–10 female flies were allowed to lay eggs for 4 d at 25°C and 75% humidity. On approximately the sixth day, wandering third-instar larvae were rinsed out of the vial and into a plastic 60 mm Petri dish. Excess water in the dish was aspirated such that the larvae remained moist but were not floating.

For thermal nociception experiments, larvae were treated and tested using a noxious heat probe (Hwang et al., 2007; Caldwell and Tracey, 2010). Briefly, the stimulus was delivered by touching the larvae laterally, in abdominal segments 4, 5, or 6. Each larva was tested only once and discarded. The response latency was measured as the time interval from the point at which the larva was first contacted by the probe until it initiated the rolling movement (the beginning of the first complete 360° roll). Statistical significance was determined using the nonparametric rank-sum Wilcoxon test.

Mechanical nociception assays were similarly performed according to Hwang et al. (2010). Briefly, wandering third-instar larvae were stimulated with a 50 mN calibrated Von Frey filament. Von Frey filaments were made from Omniflex monofilament fishing line (6 lb test; diameter, 0.009 inch [0.23 mm]). Fibers were cut to a length of 18 mm and attached to a pulled glass pipette such that 8 mm of the fiber protruded from the end and 10 mm anchored the fiber. Noxious stimuli were delivered by the rapid depression and release of the fiber on the dorsal side of a larva. A positive response was scored if at least one nocifensive roll occurred after the first stimulus. For thermal and mechanical tests, each genotype underwent three trials where at least five vials of crosses were established to obtain a sample size of ~40 larvae for a given trial. The averaged results from the trials for a given genotype were used to obtain a behavioral score and to generate the SEM, and statistical analyses were performed using the Student's *t* test.

Optogenetic activation. In cages, ~6 virgin female flies of the genotype *ppk1.9-GAL4, UAS-ChR2::eYFP; UAS-Dicer-2/K87* were crossed to 10–15 males of the desired RNAi line. VDRC lines used were *para* (6131), *spastin* (108739), and *kat-60L1* (108168). Females were allowed to lay eggs for 24 h with a dollop of yeast paste (either atr+ [500 μM] or atr−). The larval progeny were allowed to develop and feed on the yeast paste for an additional 72 h in the dark. Larvae were then stimulated with blue light (460–500 nm) with the Hg light source of a Leica MZ16 FA stereomicroscope. Blue-light pulses were manually controlled and lasted several seconds. A positive nocifensive roll was scored if the larva completed at least one revolution (360°) in response to a blue-light pulse. The averaged results from three trials for a given genotype were used to obtain a behavioral score and to generate the SEM, and statistical analyses were performed using the Student's *t* test (Honjo et al., 2012).

Gateway cloning of UAS-Venus-kat-60L1. The *kat-60L1-long* (RA) cDNA clone (accession number, AY051591) was obtained from the *Drosophila* Genomics Resource Center and amplified by PCR and gel extracted for purification. The forward primer included the ATG start site: CACCATGCGGGTCGAGGA; the reverse primer included the 5′ UTR: GGGTGCTGGGCCAGCAGCCCGTAC, and amplified a 1.84 kb product. This product was cloned into a pENTR/D-TOPO entry vector (Invitrogen) and verified by sequencing. Recombination into the pTVW

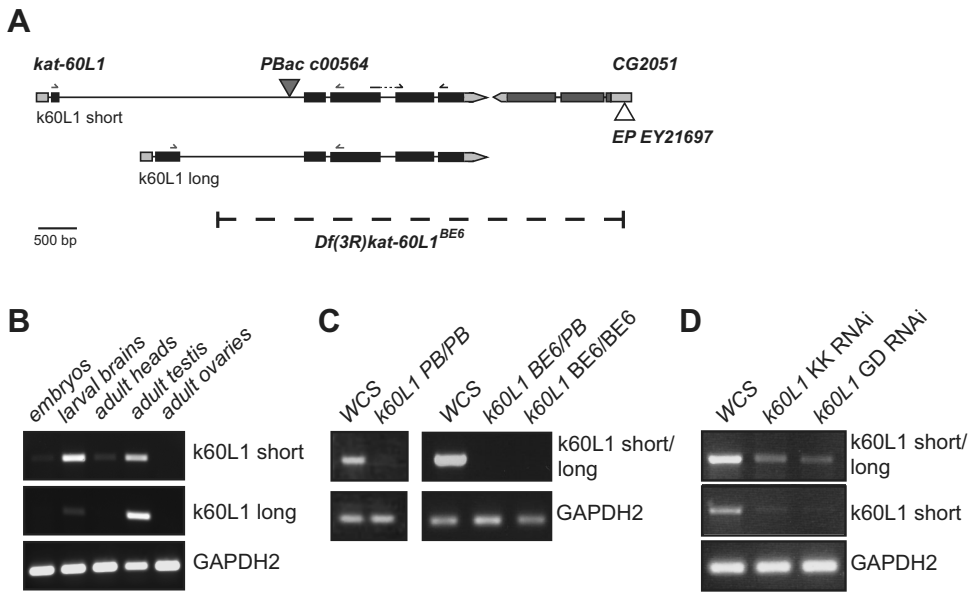

Figure 1. Molecular characterization of *kat-60L1*. ***A***, *Kat-60L1* encodes two transcripts, short (top) and long (bottom), that differ at the 5′ UTR and first exon. *PBac{PB}kat-60L1*$^{PBac\ c01236}$ (closed triangle) is inserted in the shared second intron. *P{EPgy2}CG2051*^{EY21697} (open triangle) inserted in the neighboring gene was imprecisely excised to generate *Df(3R)kat-60L1*^{BE6} (dashed line), which removes *kat-60L1* exons 2–5, the region encoding the AAA ATPase domain. Black arrows denote primers used to amplify a cDNA-specific *kat-60L1* 688 bp product. ***B***, Primers used to amplify cDNA and isoform-specific products are denoted as gray arrows in ***A*** and use a shared reverse primer. Isoform-specific RT-PCR on isolated tissues reveals strong enrichment of the short isoform in larval brains and adult testes, while the long isoform is predominantly expressed in testes, suggesting isoform-specific roles. Primers for the short isoform amplify a 344 bp product and those for the long isoform amplify a 245 bp product. ***C***, Transcript levels are strongly reduced in homozygous *kat-60L1*^{PBac} adult heads, while transcript is absent from adult heads homozygous for the *Df(3R)kat-60L1*^{BE6} allele. ***D***, Transcript levels are markedly reduced in larval brains expressing *kat-60L1* RNAi transgenes driven ubiquitously by *e22c-GAL4,sqh-GAL4*.

Gateway vector (the Drosophila Gateway Vector Collection, Carnegie Institution) was performed according to the manufacturer's instructions. The final N-terminal Venus-tagged *kat-60L1-long* vector *UAS-Venus-kat-60L1* was sent to the Duke University Model Systems Genomics Core for injection and fly transformation (Durham, NC).

Immunohistochemistry. Antibodies used were mouse anti-GFP (1:500; Invitrogen), mouse anti-Futsch 22C10 (1:500), and mouse anti-acetylated Tubulin (1:500; both from Developmental Studies Hybridoma Bank). Alexa-Fluor 488 or 568 fluorescent secondary antibodies (Invitrogen) were used at 1:200. Whole-mount immunohistochemistry on embryos was performed according to standard techniques. Larvae were filleted by opening the ventral side in HL3 Ringers solution, followed by fixation for 40 min in 4% paraformaldehyde (Electron Microscopy Sciences). The larvae were then rinsed three times and washed 3 × 15 min in PBST (0.2% Triton-X) and blocked with PBTNA (10% normal goat serum, 1% BSA, and 0.01% azide in 0.2% PBST) for 1 h. Antibody solutions were prepared in PBTNA and the larvae were incubated with primary antibody for either 3 h at room temperature or overnight at 4°C, rinsed three times, and washed 3 × 15 min in PBST. Secondary antibodies were incubated with samples for either 2 h at room temperature or overnight at 4°C and then washed as for the primary antibodies. Samples were mounted in Vectashield (Vector Laboratories) for imaging.

Neuron visualization and analysis. Visualization of neuron morphology was performed as described by Grueber et al. (2002), then analyzed either manually or by NeuronJ, a plugin of ImageJ software (Meijering et al., 2004). Images were collected on a Zeiss 510 confocal microscope and converted to maximum intensity projections of *z*-stack images using LSM Image Browser software, and brightness and contrast were adjusted using Adobe Photoshop. One or two neurons per larva from abdominal segments 3 or 4 were used for visualization and analysis and at least five individual larvae per genotype were used for each set of analyses. The total number of terminal dendritic branches was assessed by manual counts to address the degree of branching. Terminal branch length was measured using the trace function in NeuronJ. Dendritic coverage was quantified in ImageJ by overlaying a grid of squares, each ~0.12% of the total average arbor size, over the arbor and calculating the number of boxes containing only white space as a percentage of total box number. Strahler analysis was conducted to assess branching complexity across orders of branches. Branches were ordered and quantified, with the most distal branches from the cell body (terminal) denoted 1 and those approaching the cell body (primary branches) ordered consecutively, up to 6, terminating at the cell body. For the developmental time course, embryos were collected on grape juice plates from overnight collections and newly hatched first-instar larvae of both genotypes were synchronized for staging at 25°C. Beginning at the second-instar stage, larvae were collected at the appropriate time point and imaged by confocal microscopy.

Live imaging and analysis of branching events in anesthetized larvae. Third-instar larvae were anesthetized under 90% glycerol for ~10 min in an enclosed Petri dish containing 1–2 ml of ether applied to a cotton ball. Anesthetized larvae were then transferred to a slide containing halocarbon oil 27 and a coverslip was gently depressed dorsally. Dorsal cluster class IV neurons from segments 3–6 were imaged on a Zeiss LSM 5 LIVE confocal microscope using a 40×, 1.3NA Plan-Neofluar oil immersion objective. *Z*-stack images of terminal branches near the dorsal midline were collected approximately every 30 s for 15–30 min time periods. *Z*-stack time series were converted into maximum intensity projection time series using Zeiss LSM imaging software. To quantify branching events, six late, wandering third-instar and five early (before wandering) third-instar larvae per genotype were analyzed for 10 consecutive minutes (>500 branches per genotype were scored). Each branch was marked as either stable, or undergoing a dynamic extension, retraction, or extension/retraction (fluid) event over the 10 min interval. A branch was scored as dynamic only if the branch could be tracked as moving for >1 μm distance. Percentages were calculated for each branching category and the SD was calculated across total larvae. Statistical significance was determined using the Student's *t* test.

Live imaging of EB1-labeled microtubules. All imaging of da neurons was performed on intact third-instar larvae mounted on a dried agarose pad under a coverslip. Third-instar larvae were selected for imaging but were smaller than late, wandering third-instar larvae because smaller animals allowed for improved visualization of so-called "comets," the concentrated pools of exchanging EB1-GFP at growing microtubule tips. Neurons were imaged using a 63× oil objective on a Zeiss Axiovision confocal microscope or a Zeiss 510 confocal microscope and images were

recorded every 1 s for 200 cycles. Movies were analyzed using ImageJ software. An EB1-labeled comet was counted only if it was detectable and tracked in consecutive frames for at least 7 s.

Results

Kat-60L1 short and long isoforms are differentially expressed throughout development

Several lines of evidence support a role for Kat-60L1 in the *Drosophila* nervous system. Embryonic *in situs* made available by the Berkeley *Drosophila* Genome Project show *kat-60L1* mRNA expression localized to sensory organs and neurons, the brain, and the ventral nerve cord (VNC; Tomancak et al., 2002). Fly Atlas, the *Drosophila* adult gene expression database, also reveals fourfold enrichment of *kat-60L1* transcript in the adult brain and VNC, as well as eightfold in adult testis, relative to the whole animal (Chintapalli et al., 2007). The role of Kat-60L1 in these adult tissues has not been investigated.

To further understand the expression of Kat-60L1, we performed tissue-specific RT-PCR. *Kat-60L1* encodes a short (605 aa) and long (669 aa) isoform: the 5′ UTR of the long isoform initiates from within the second intron of the short isoform, while exons 2–5, which include the AAA ATPase (ATPase associated with diverse cellular activities) catalytic domain, are identical (Fig. 1*A*). These two *kat-60L1* isoforms were expressed differentially across the tissues examined and, therefore, likely play distinct roles (Fig. 1*B*). Transcript for the short isoform was highly enriched in third-instar larval brains, at intermediate levels in adult testes, and at low levels in stage 11–17 embryos and adult heads. Neither isoform was expressed in the adult ovary, consistent with adult Fly Atlas results. In contrast, the long isoform was highly enriched in adult testes but expressed only at low levels in third-instar larval brains, and was not detectable in embryos or in adult brains. *Kat-60L1-short* is thus the predominant isoform in the larval nervous system and throughout nervous system development, albeit at lower levels in embryos and adults.

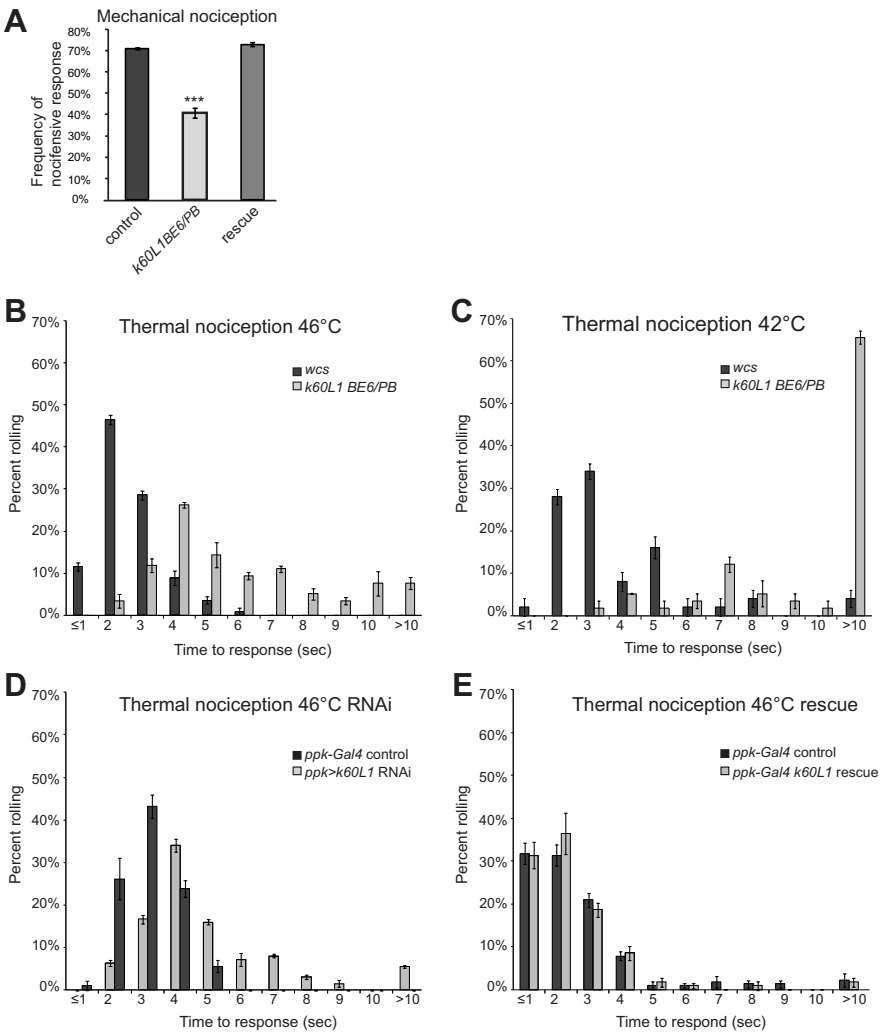

Figure 2. Kat-60L1 is necessary for proper nocifensive responses. ***A***, Mechanical nociception assay. Control larvae subjected to a noxious mechanical force display an escape roll 70% of the time, whereas *kat-60L1*$^{BE6/Pbac}$-mutant larvae roll only 40% of the time ($n > 76$; $p < 1 \times 10^{-4}$). Rescue animals display an avoidance response indistinguishable from controls ($n > 180$; $p < 1 \times 10^{-4}$ compared with mutants). ***B–E***, Thermal nociception assay. ***B***, *kat-60L1*$^{BE6/Pbac}$-mutant larvae subjected to a high-temperature thermal probe of 46°C take significantly more time to exhibit an escape response, as seen by their right-shifted distribution compared with *WCS* controls ($n = 3$ trials, >110 larvae; $p < 1 \times 10^{-4}$). ***C***, Mutants are also significantly delayed in the NEL response compared with *WCS* controls at the lower threshold temperature of 42°C ($n = 3$ trials, >50 larvae; $p < 1 \times 10^{-4}$). ***D***, Specific expression of *kat-60L1* RNAi in class IV da neurons phenocopies *kat-60L1*$^{BE6/PBac}$ insensitivity to noxious heat compared with *ppk1.9-GAL4; Dicer2* controls ($n = 3$ trials, >85 larvae; $p < 1 \times 10^{-4}$). ***E***, Specific expression of *Venus-kat-60L1*^{14} in class IV da neurons in the *kat-60L1*$^{BE6/Pbac}$-mutant background rescues the thermal insensitivity phenotype to control levels ($n = 3$ trials, >115 larvae; $p > 0.05$). In this and all subsequent figures, error bars indicate the SEM; *p* values are calculated using a Student's *t* test except for thermal nociception experiments, which were calculated using a nonparametric rank-sum Wilcoxon test, and $*p < 0.05$, $**p < 0.01$, $***p < 0.001$.

Characterization of *kat-60L1* loss-of-function alleles

We next sought to identify mutant alleles for *kat-60L1* with the goal of investigating its *in vivo* functions. We began with an available piggyBac insertion (*katanin p60-Like 1*$^{PBac\ c01236}$, hereon referred to as *kat-60L1*^{PBac}; Thibault et al., 2004). This insertion is located in the second intron of *kat-60L1*, which is common to both isoforms (Fig. 1*A*). Notably, this allele showed highly reduced, but still detectable transcript levels (Fig. 1*C*). Adults homozygous for the mutation appeared healthy and, unlike *spastin* mutants (Sherwood et al., 2004), did not exhibit defects at the larval neuromuscular junction (data not shown). We also characterized *kat-60L1* RNAi lines made available by the Vienna *Drosophila* RNAi Center by crossing *UAS-RNAi* animals to a *GAL4* driver with ubiquitous promoter expression *e22c-GAL4, sqh-GAL4* (Franke et al., 2010). RT-PCR of third-instar larval brains showed strong, albeit incomplete, reduction of *kat-60L1* transcript levels in all RNAi samples, compared with wild-type controls (Fig. 1*D*).

Because small amounts of transcript may be sufficient for Kat-60L1 function, we reasoned that the above alleles might not uncover all of the endogenous requirements for Kat-60L1. We therefore generated a genetic deletion of *kat-60L1* by imprecise

excision of P-element *EY21697*, which is located in the 5′ UTR of *CG2051,* an uncharacterized gene immediately distal to *kat-60L1* on the right arm of chromosome 3 (Fig. 1*A*). We recovered one excision, denoted *Df(3R)kat-60L1*^{BE6}, or *BE6*, that deletes from the second intron of *kat-60L1* to the 5′ UTR of *CG2051*, removing the majority of *kat-60L1* and the entire coding sequence of *CG2051* (Fig. 1*A*). RT-PCR using primers spanning exons 3–5 confirmed that this region of *kat-60L1* transcript is absent in a homozygous *BE6* background. Compared with the homozygous *kat-60L1*^{Pbac} brains, transcript was undetectable in the brains of trans-heterozygous *BE6/PBac* animals (Fig. 1*C*); thus, we preferentially used this background throughout the study. The use of the transheterozygous allelic combination also enabled us to reduce the potential effects of second-site mutations in the genetic background of each unique allele, and to cover the *CG2051* deletion in *Df(3R)kat-60L1*^{BE6}. Animals homozygous for the *BE6* deletion, as well as *kat-60L1*$^{BE6/PBac}$ transheterozygotes, survived to adulthood but exhibited a reduced lifespan, with 49% of the *kat-60L1*$^{BE6/PBac}$ population dying by 2 weeks after eclosion. This was dramatically different from the 2.5% mortality seen in wild-type controls ($n > 37$).

Kat-60L1-short is necessary for proper nocifensive responses mediated by class IV da sensory neurons

The class IV da neurons are polymodal nociceptors that mediate mechanical and thermal nocifensive responses (Hwang et al., 2007). We used a mechanical nociception assay to determine whether *kat-60L1* mutations affect the function of class IV neurons. In this assay, larvae are delivered a harsh touch by depressing the dorsal body wall with a 50 mN Von Frey fiber (Tracey et al., 2003). Wild-type larvae typically (70% of animals) responded to this stimulus with nocifensive escape locomotion (NEL), in which the animal rotates around its long body axis. In contrast, *kat-60L1*$^{BE6/PBac}$ larvae responded less frequently to the noxious mechanical stimulus, exhibiting NEL only 40% of the time (Fig. 2*A*).

To pinpoint whether this mechanical nociceptive defect originates in the class IV da neurons, we used the *GAL4-UAS* system (Brand and Perrimon, 1993) to induce tissue-specific expression of *kat-60L1-RNAi*, as well as *Dicer2* (Dietzl et al., 2007), under the control of *ppk1.9-GAL4*, which drives expression uniquely in the class IV neurons (Ainsley et al., 2003). Notably, this manipulation phenocopied the *kat-60L1*$^{BE6/PBac}$ mutants ($p < 1 \times 10^{-4}$ compared with their matched controls; $n > 130$), indicating that loss of Kat-60L1 solely in class IV da neurons reduces mechanical nociceptive responses to levels equivalent to the genetic loss-of-function mutant.

Because class IV neurons are polymodal nociceptors, we tested whether the *kat-60L1* defects are modality-specific by assaying *kat-60L1*$^{BE6/PBac}$ mutant larvae for their response to noxious heat, also mediated by the class IV da neurons (Hwang et al., 2007). Wild-type third-instar larvae touched with a high-temperature probe of 46°C initiated NEL within the first 2–3 s of stimulation. In contrast, *kat-60L1*$^{BE6/Pbac}$-mutant larvae were severely delayed in their response, often requiring up to 10 s (Fig. 2*B*). This insensitivity was maintained at a lower threshold temperature of 42°C, indicating an overall failure to respond to noxious temperatures (Fig. 2*C*). Class IV neuron-specific RNAi knockdown of *kat-60L1* expression again phenocopied the *kat-60L1* genetic mutant results, providing further evidence that the site of action for Kat-60L1 in regulating this behavior is localized to this neuronal subset (Fig. 2*D*).

To further confirm that the mutations in *kat-60L1* were responsible for the observed nociceptive phenotypes, we generated an N-terminal Venus-tagged *UAS-kat-60L1* rescue transgene. *kat-60L1*$^{BE6/PBac}$ larvae that also expressed the short isoform cDNA transgene specifically in class IV neurons were assayed for rescue of the *kat-60L1*-mutant behavior phenotypes. In both thermal and mechanical nociceptive assays, these larvae displayed nocifensive responses indistinguishable from controls (Fig. 2*A*,*E*). Together, these data demonstrate that mutations in *kat-60L1* underlie the observed defects in larval nociception. Furthermore, this requirement for *kat-60L1* is specifically in the class IV da neurons.

Kat-60L1 is required for the complex dendritic morphology of class IV neurons

To understand the cell biological defects underlying compromised class IV neuron function in *kat-60L1* mutants, we examined the dorsal cluster dendritic arbors marked with *ppk1.9-GAL4, UAS-mCD8::GFP* in the *kat-60L1*$^{BE6/PBac}$ background (Fig. 3*A–C*). Class IV dendrite arbors normally exhibit complex branching and extensive coverage of the overlying epidermal wall. Loss of *kat-60L1* resulted in large gaps, both between neighboring class IV dendritic arbors and within the arbor of an individual neuron. We measured dendrite arbor coverage of each neuron by using an overlaid grid of 250 μm^2 squares (Fig. 3*D*; Jinushi-Nakao et al., 2007) to quantify the area that lacked any portion of a dendrite branch (white space). *kat-60L1* loss-of-function larvae showed a 26% reduction in the grid squares containing dendrite segments compared with control neurons, which showed dendrites in 98% of the squares in the grid. To determine the source of the reduced coverage, we counted the number of dendrite termini in the class IV da neuron arbors and observed a 22% reduction in *kat-60L1*$^{BE6/PBac}$ mutants compared with controls (Fig. 3*E*). Average lengths of dendrite termini exhibited a 29% decrease in *kat-60L1*$^{BE6/PBac}$ mutants compared with controls (Fig. 3*F*,*A–C,* insets).

Although terminal branches appeared most affected, closer examination of branching patterns using Strahler analysis (Grueber et al., 2002) revealed an overall reduction of branches in more proximal regions as well. *kat-60L1*$^{BE6/PBac}$ mutants exhibited a significant reduction of branches in all orders except for those most proximal (near the cell body), compared with controls (Fig. 3*G*). Knockdown of *kat-60L1* specifically in class IV neurons by RNAi resulted in a similar reduction of dendritic outgrowth compared with controls, albeit not as severe as the genetic mutants (data not shown). Kat-60L1 thus regulates both branch number and length of class IV dendrites to establish complete coverage of the overlying epidermis. Expressing a single copy of *UAS-Venus-kat-60L1*^{14} specifically in class IV neurons of *kat-60L1*$^{BE6/PBac}$ larvae completely restored dendritic arbor morphology (Fig. 3*C–G*), confirming that loss of *kat-60L1* within these neurons is responsible for the observed mutant phenotypes.

To determine whether the morphological defects were specific to the dendritic compartment, we observed class IV axonal projections, which extend from the cell body near the larval epithelium to the VNC in the CNS. In the VNC, the axonal projections form a ladder-like pattern due to innervation of longitudinal tracts and contralaterals that cross the midline via commissures (Grueber et al., 2007). *ppk1.9-GAL4, UAS-mCD8::GFP*-labeled axons within the VNC in *kat-60L1*$^{BE6/Pbac}$-mutant animals showed no gross alterations in the appearance of commissures or the longitudinal axon tracts compared with controls (Fig. 3*H*), suggesting that the *kat-60L1* loss-of-function defects are specific to the regulation of the dendritic arbors. Together, these data suggest that Kat-60L1 is not required for the axonal projection of

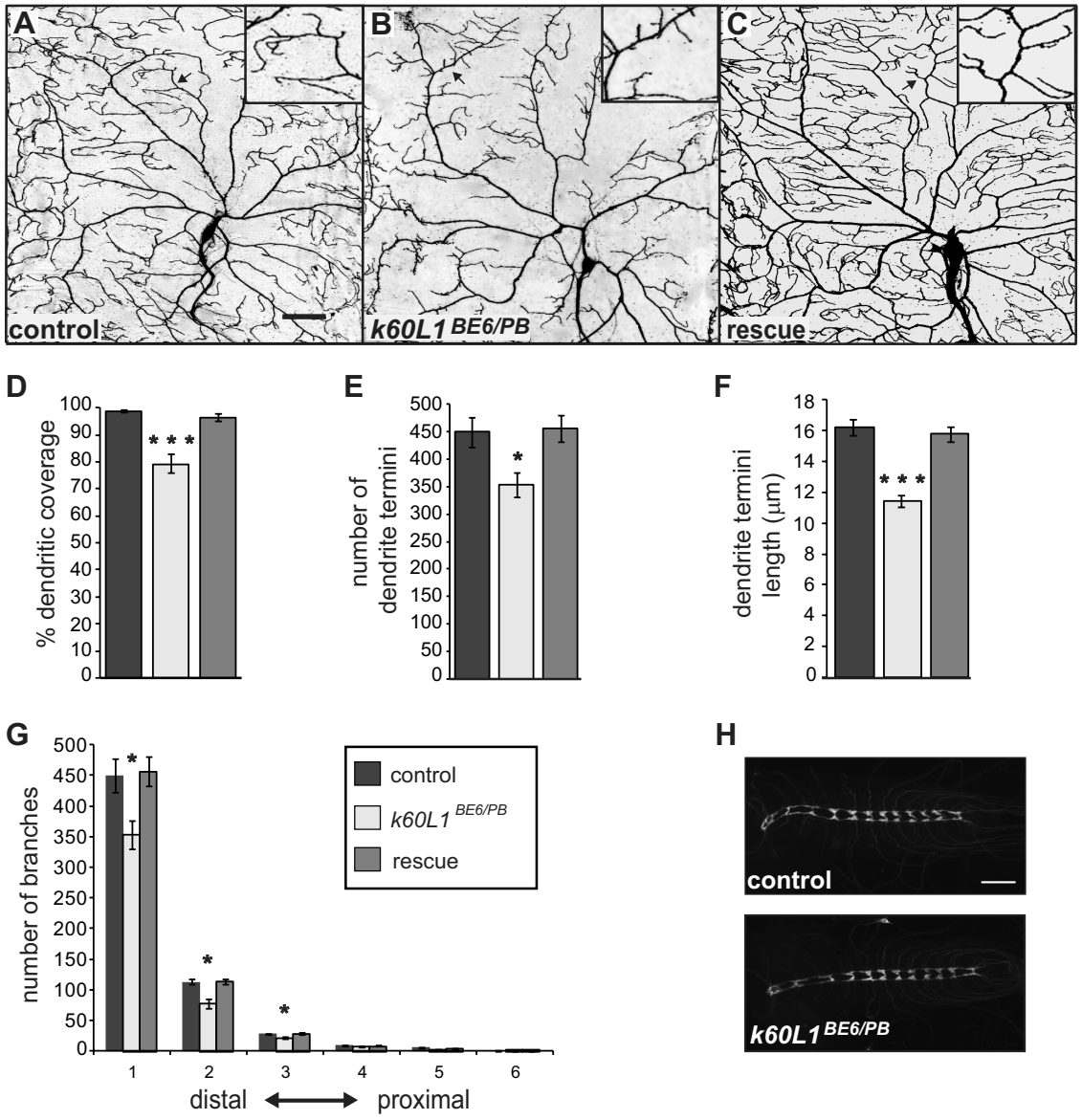

Figure 3. Loss of *kat-60L1* decreases dendritic branch number, length, and arbor coverage in class IV neurons. ***A–C***, Comparison of *kat-60L1*-mutant and control dorsal cluster class IV da neurons from wandering third-instar larvae in a *ppk1.9-GAL4, UAS-mCD8::GFP/+* background. Representative arbors from (***A***) control, (***B***) *kat-60L1*$^{BE6/PB}$-mutant, and (***C***) *kat-60L1*-genetic-rescue larvae. ***D–G***, Comparison of (***D***) dendritic field coverage ($n = 8$ arbors per genotype; $p < 1 \times 10^{-4}$), (***E***) total terminal branch number ($n > 5$ arbors; $p < 0.02$), (***F***) terminal branch length ($n > 735$ branches from > 5 arbors; $p < 1 \times 10^{-4}$), and (***G***) dendritic arbor complexity as measured by Strahler analysis between control, mutant, and rescue animals ($n > 5$ arbors; $p < 0.02$ for all orders). ***H***, Representative images of *ppk1.9-GAL4, UAS-mCD8::GFP*-labeled axons in third-instar larval VNCs from control (top) and *kat-60L1*$^{BE6/PB}$-mutant (bottom) larvae appear identical. Scale bars, 50 μm.

larval class IV da neurons, but it is required to establish their highly branched dendritic arbor and mediate their nocifensive functions.

Kat-60L1 is required during late larval stages for class IV dendrite arbor outgrowth

When might Kat-60L1 be required for the establishment of the class IV dendritic arbor? Kat-60L1 could function throughout dendritic development or only at one or more discrete developmental time points. To distinguish between these possibilities, we conducted a developmental time course of arbor morphology. Class IV neuron dendrites begin branching during mid-embryogenesis, ~16 h after egg lay (AEL), growing rapidly in the late embryo and early larva to establish dendritic tiling of the body wall by 48 h AEL. Between 48 h AEL (the second-instar stage) and 120 h AEL (just before metamorphosis), larvae triple in body length, and complete coverage of the dorsal area (which increases sixfold) by class IV arbors is maintained correspondingly. Thus, this latter process, referred to as dendritic scaling, also requires rapid branching (Parrish et al., 2009).

We compared dendritic arbors of *kat-60L1* mutants to wild-type controls from early second-instar larvae (48 h AEL) just at the beginning of the dendritic scaling phase, early third-instar larvae (72 h AEL) in the middle of this phase, and late wandering third-instar larvae (120 AEL), which should exhibit fully formed dendritic arbors. Boxes of the grids overlaid on dendrite arbors at the different stages were scaled in size relative to the entire arbor so that each box represented ~0.12% of the total area. At 48 h AEL, *kat-60L1* mutants showed slightly lower average dendritic coverage compared with controls (89 vs 93%; Fig. 4*A*, *A*',*D*), indicating a minor role for Kat-60L1 in dendrite outgrowth be-

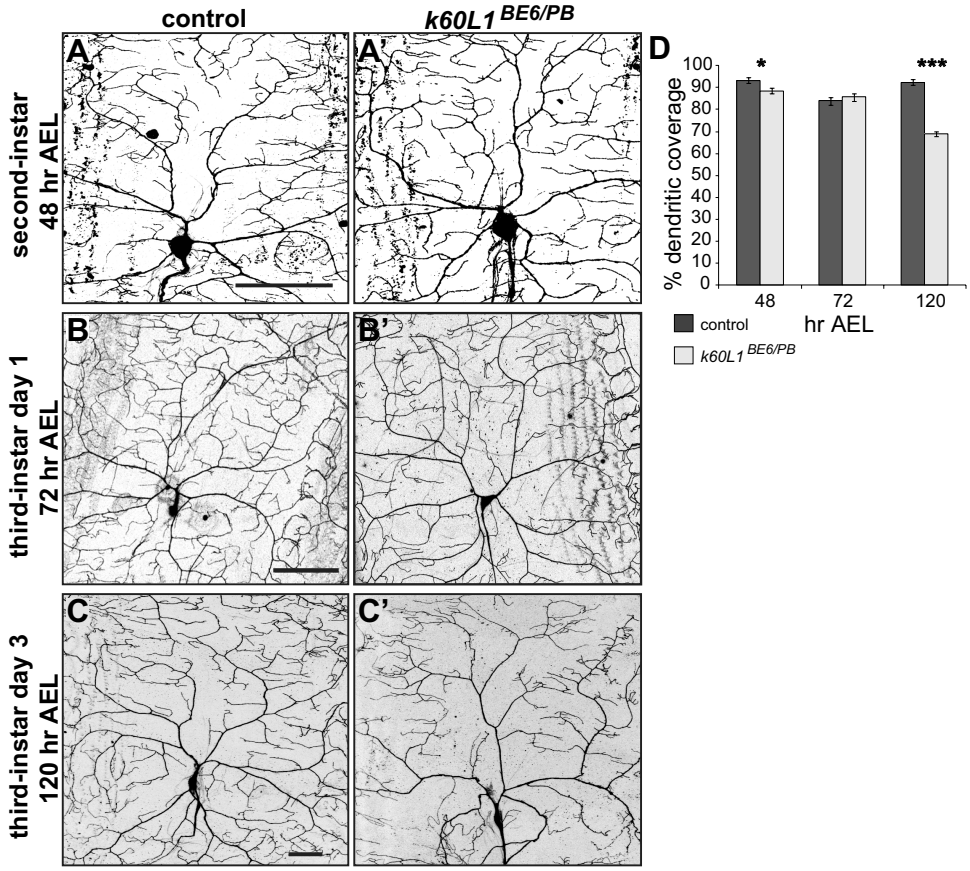

Figure 4. Kat-60L1 is required for late larval development of class IV da neuron dendrites. ***A–C′***, Confocal images of class IV dendritic arbors from control (***A–C***, left) and *kat-60L1*$^{BE6/Pbac}$-mutant (***A′–C′***, right) larvae. Representative arbors from (***A***) second-instar, (***B***) day one third-instar, and (***C***) day three third-instar larvae. ***D***, Dendritic coverage measured from 48 to 120 h AEL for *kat-60L1*$^{BE6/Pbac}$-mutant and control larvae shows a strong reduction in mutants late in larval development ($n > 5$ arbors per genotype; $p < 0.05$, $p > 0.5$, $p < 1 \times 10^{-4}$, for 48, 72, and 120 h, respectively). Scale bars, 50 μm.

fore the scaling phase. Twenty-four hours later during the first day of the third-instar stage, however, no significant difference in dendritic coverage was observed in mutant larvae compared with controls (Fig. 4*B*,*B*',*D*). Mutants were thus able to compensate for the earlier difference and establish full coverage, as well as maintain scaling growth, during this period. By the late-wandering third-instar stage, however, morphological differences were equivalent to the *kat-60L1*$^{BE6/Pbac}$-mutant dendrite arbors reported above, with *kat-60L1* mutants displaying on average only 69% coverage, compared with 93% coverage in controls (Fig. 4*C*,*C*',*D*). These data demonstrate that Kat-60L1 is not required for initial dendritic branch formation in the larva, but rather for arborization after 72 h AEL during third-instar larval development. Different branches of the dendritic arbor thus have distinct requirements for their formation.

Kat-60L1 is required to stabilize nascent terminal dendrites

To further understand how dendritic branches fail to form properly during late third instar in *kat-60L1*-mutant animals, we performed time-lapse imaging of branching events in live, intact animals. We hypothesized that class IV arbors lacking Kat-60L1 fail to stabilize their terminal branches successfully due to a lack of microtubule invasion following the initial step of filamentous-actin-based protrusion to create nascent branches (Moore, 2008). This predicts that *kat-60L1* arbors, lacking microtubule stability, would display either less branch formation or unstable branching compared with controls. Wandering, late third-instar animals either wild-type or mutant at the *kat-60L1* locus and expressing *ppk1.9-GAL4, UAS-mCD8::GFP* to label class IV neurons were anesthetized and continuously imaged via confocal for 15–30 min. Control larvae at this stage exhibited relatively stable terminal branches, with few rapid branching events (Fig. 5*A*). In contrast, *kat-60L1* larvae exhibited highly dynamic branching events. Terminal branches frequently extended (Fig. 5*B,* yellow arrowheads), retracted (Fig. 5*B,* blue arrows), or extended and retracted within a 15–30 min time period in *kat-60L1* mutants. We quantified the branching events by analyzing 10 consecutive minutes of time-lapse movies every 30 s. Every branch in the field was observed over time and marked as a stable (Fig. 5*C*,*D,* small red circles), extension (Fig. 5*C*,*D,* yellow arrowheads), retraction (Fig. 5*C*,*D,* blue squares), or extension/retraction ("fluid"; Fig. 5*C*,*D,* large green circles) branch event. The majority of branches were stable in control arbors, with only 31 $\pm$ 7.1% extending or retracting, while *kat-60L1*-mutant arbors had on average nearly twice as many dynamic branches (58 $\pm$ 8.4%; $p < 0.03$; Fig. 5*E*). Regardless of whether the dynamic events were extensions, retractions, or fluid events, all occurred more frequently in mutant arbors compared with controls (Fig. 5*E*).

In contrast to late third-instar stage control dendrites, early third-instar control dendrites were highly dynamic (58 $\pm$ 9.3%), and no difference in branching events was observed compared with *kat-60L1* mutants at the same stage (60 $\pm$ 8.7% dynamic branches; $p > 0.8$). Terminal branches are therefore predominantly dynamic at early third instar, and stabilize as larval devel-

opment progresses. Furthermore, while Kat-60L1 does not play an obvious role in these early terminal branch dynamics, it is required for their subsequent stabilization.

Kat-60L1 promotes microtubule growth in class IV dendritic arbors

Given Kat-60L1's role in promoting late-stage dendrite stability together with its proposed function as a microtubule-severing protein, we examined whether Kat-60L1 regulates microtubules within dendrites at this stage. Using an antibody directed against the *Drosophila* MAP1B ortholog Futsch, a neuron-specific microtubule-binding protein and a marker of stabilized microtubules, we observed no difference in the intensity or distribution of this microtubule population between *kat-60L1* mutants and wild-type controls (data not shown). However, Futsch immunostaining is not detected in first-order (terminal) and some second-order branches, where the most striking *kat-60L1* phenotypes are observed. Similarly, immunostaining of the stable, acetylated microtubule population failed to reveal any difference between genotypes, but also labeled only relatively proximal branches (data not shown). These results suggest that stabilized microtubules within da neurons are localized proximally in the cell and are not grossly affected by loss of Kat-60L1.

Because immunostaining of stable microtubule populations failed to label the terminal branches most affected in *kat-60L1* mutants, we examined the dynamic population of microtubules within the class IV arbors by imaging the microtubule plus-end tracking protein EB1 in living whole-mounted third-instar larvae (Stone et al., 2008). EB1 proteins exchange rapidly at growing microtubule tips (Zanic et al., 2009), thus providing a highly sensitive marker of individual growing filaments. The concentrated pools of exchanging EB1-GFP at growing microtubule tips appear as bright "comets" and can be visualized and tracked along polymerizing microtubules. *EB1-GFP* was expressed using the class IV-specific *477-GAL4* driver, which drives expression at a lower level compared with *ppk1.9-GAL4* (Williams et al., 2006). Moderate expression of EB1-GFP is required to distinguish individual comets among the background of unbound EB1-GFP in branches. Although terminal branches were difficult to visualize and rarely exhibited comets, comets were clearly observed in the distal secondary and tertiary branches adjacent to terminal branch points. Strikingly, we found that, in these branches, *kat-60L1*$^{BE6/PBac}$ mutants exhibited fewer than half as many EB1 plus-end comets compared with controls (Fig. 6). We quantified the number of comets over branch length and found on average 0.32 ± 0.01 comets/μm in branches of control animals and 0.15 ± 0.01 comets/μm in those of *kat-60L1*-mutant animals ($p < 1 \times 10^{-4}$; $n > 95$ comets in ≥6 larvae per genotype). In contrast, average comet speed did not differ, moving 0.1 μm/s in both genotypes ($p > 0.15$), values consistent with speeds observed previously (Mattie et al., 2010). Furthermore, there was no difference between genotypes in the number of EB1-GFP comets in the

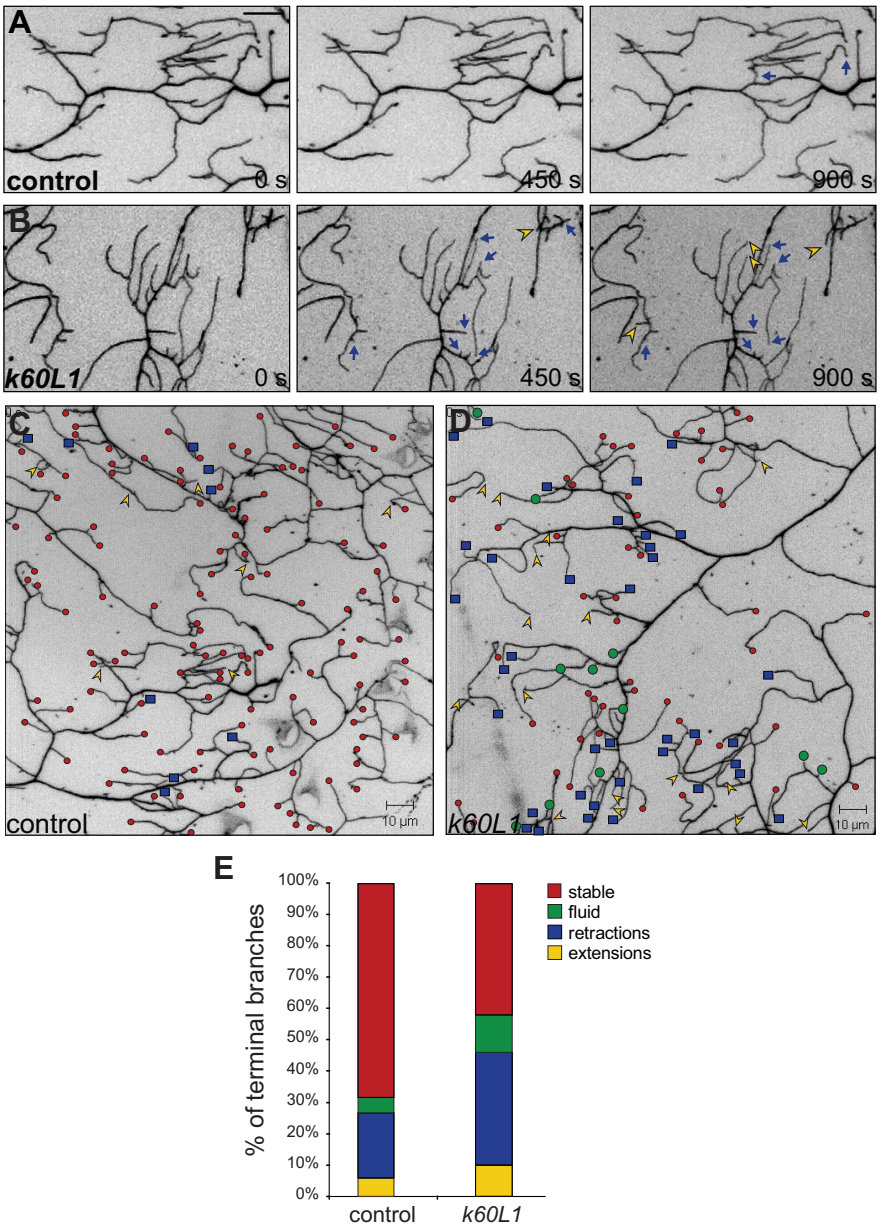

Figure 5. Kat-60L1 promotes terminal branch stabilization. ***A***, ***B***, Branching dynamics, revealed by time-lapse confocal images over 450 s intervals, of class IV dendritic terminals expressing *ppk1.9-GAL4, UAS-mCD8::GFP*. Scale bar, 10 μm. ***A***, A representative control larva exhibits relatively stable branches over a 15 min period. Only a few branches undergo retraction events (blue arrows). ***B***, In contrast, a representative *kat-60L1*-mutant larva exhibits multiple dynamic branching events, including retractions (blue arrows) and extensions (yellow arrowheads). ***C***, ***D***, Composite of stable versus dynamic events in class IV terminal branches, analyzed from time-lapse movies imaged at 30 s intervals for 10 min. Stable branches are represented by small red circles, retractions by blue squares, extensions by yellow arrowheads, and branches that both extend and retract (fluid) by large green circles. A control larva (***C***) exhibits many stable branches and few dynamic branching events, while a *kat-60L1* mutant (***D***) exhibits many dynamic branching events and fewer stable branches, as well as fewer overall terminal branches. ***E***, Bar graph depicting the relative percentages of stable and dynamic branching events from control and *kat-60L1*-mutant larvae. Note the nearly twofold increase for all dynamic branching events (retractions, extensions, and fluid) in *kat-60L1*-mutant animals (total dynamic, 58 ± 8.4%) compared with controls (total dynamic, 31 ± 7.1%; $n = 6$ larvae and >600 branches analyzed per genotype; $p < 0.03$).

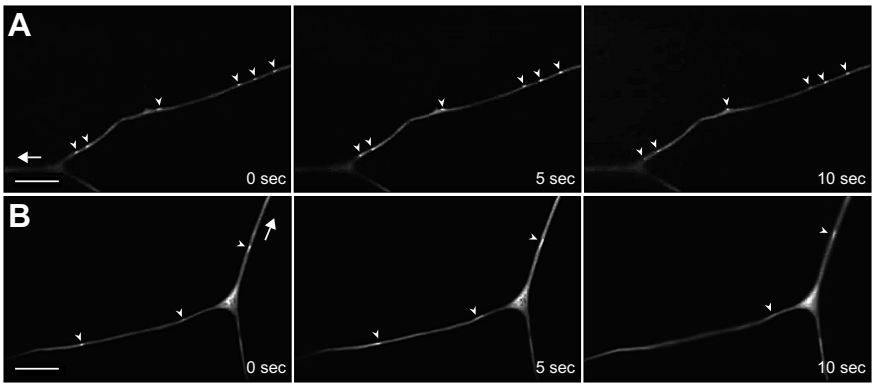

Figure 6. The number of growing microtubules is reduced in *kat-60L1* dendrites. ***A***, ***B***, Representative time-lapse images of EB1::GFP comets (arrowheads) in class IV dendrites of (***A***) control and (***B***) *kat-60L1*$^{BE6/PBac}$ third-instar larvae. Images were collected at 63× magnification over consecutive 5 s intervals. Arrow depicts the direction of the cell body, toward which most EB1 comets travel. Scale bar, 5 μm.

axons of these neurons, which averaged ~1/120 μm ($n > 6$ neurons per genotype; $p > 0.8$) in the proximal axon adjacent to the cell body. Together, our live imaging data support a novel role for Kat-60L1 in upregulating the number, but not the rate, of growing microtubules in the dendrites of class IV neurons, thereby promoting branch stabilization of the dendritic arbor during third-instar larval development. Moreover, the effect of Kat-60L1 on microtubule dynamics is specific to dendrites, and is not seen in the axon.

Kat-60L1 is required specifically in dendrites, distinct from Spastin

Previous work from others has shown that partial loss or gain of the microtubule-severing protein Spastin also results in class IV dendrites with reduced complexity (Jinushi-Nakao et al., 2007; Ye et al., 2011). We therefore asked whether the functions of Kat-60L1 in the larval class IV dendrites are unique, or a general function of microtubule-severing proteins in these neurons. Based on their similar morphological phenotype, we first predicted that, like *kat-60L1* mutants, reduced Spastin levels should lead to nocifensive defects. Indeed, animals deleted for one copy of fly *spastin*, *spastin*$^{5.75/+}$ larvae, exhibited comparable insensitivity to noxious mechanical stimuli, with *WCS* control larvae displaying an escape response 73% of the time, but *spastin*$^{5.75/+}$-mutant larvae rolling only 58% of the time ($p < 1 \times 10^{-4}$). Responses to thermal nociceptive stimuli were also reduced in *spastin*$^{5.75/+}$ mutants, which exhibit similarly compromised arbor morphology as *kat-60L1* mutants (Fig. 7*A*; Jinushi-Nakao et al., 2007). These data further support the notion that the full dendritic complexity of the class IV neurons is required for proper nocifensive responses.

Unlike Kat-60L1, however, Spastin is required not only for complete dendrite arborization (Jinushi-Nakao et al., 2007), but also for da neuron axon elaboration in the VNC (Ye et al., 2011). Thus, the behavioral defects in *spastin* mutants could result from the dendritic morphology perturbations, the axonal defects, or both. In contrast, Kat-60L1 affected dendrites without altering the gross morphology of the central projections of the class IV da neurons, suggesting that the dendrite phenotype alone is responsible for the severe nociception defects of Kat-60L1 mutants.

To further elucidate the *spastin* and *kat-60L1* loss-of-function phenotypes, we tested the effects of each mutation on optogenetically triggered NEL. Exposure of animals expressing channelrhodopsin-2YFP (ChR2::eYFP) under the control of *ppk1.9-GAL4* to blue light depolarizes class IV da neurons and triggers NEL (Hwang et al., 2007). The optogenetically activated NEL response bypasses normal sensory transduction mechanisms, but still requires downstream factors such as the voltage-gated sodium channel Para, which is required for the action potential (Siddiqi and Benzer, 1976; Wu and Ganetzky, 1980; Zhong et al., 2010). In control larvae expressing ChR2::eYFP in class IV nociceptors, robust NEL behavior was seen in 69% of animals in response to blue-light illumination. Consistent with previous studies (Zhong et al., 2010), this was reduced to 21% when *para* RNAi was simultaneously expressed (Fig. 7*B*). When we instead knocked down *kat-60L1* by RNAi within class IV neurons, ChR2::eYFP-triggered escape behavior was unaffected (Fig. 7*B*), indicating that Kat-60L1 activity is not necessary for steps downstream of sensory transduction. In comparison, knockdown of *spastin* by RNAi, or genetic removal of one copy of *spastin*, both caused a reduction in ChR2::eYFP-triggered NEL that was comparable to knockdown of *para*. Spastin loss therefore causes neuronal defects that cannot be overcome by bypassing normal nociceptive transduction mechanisms, consistent with a functional requirement for Spastin in both somatodendritic and axonal compartments of the class IV sensory neurons. Kat-60L1 activity, in contrast, is required upstream at the level of the dendrite or cell body, and not for general excitability and presynaptic function in these sensory neurons.

Kat-60L1 regulates dendritic microtubules in class IV neurons through mechanisms distinct from Spastin

To find out whether the functional differences between *kat-60L1* and *spastin* in class IV neurons are due to differences in their subcellular site(s) of action or whether they have distinct effects on microtubules, we examined EB1-GFP comets in *spastin* loss-of-function mutants. In striking contrast to *kat-60L1* mutants (Fig. 5), *spastin*$^{5.75/+}$ dendrites showed no change in the number of comets compared with controls, despite their similarly reduced arbors (0.31 comets/μm vs 0.29 comets/μm, $p > 0.4$). This suggests that Spastin does not promote microtubule growth in dendrites and instead regulates microtubules in a manner distinct from Kat-60L1.

We further investigated the activities of Kat-60L1 and Spastin on microtubules by overexpressing each protein. Spastin overexpression in class IV neurons dramatically reduced Futsch-labeled microtubules in these cells (Fig. 8, compare *B3*, *A3*). Neighboring neurons not overexpressing *spastin* served as internal controls and were consistently Futsch-positive. In contrast, when *kat-60L1* was ectopically expressed within these cells, we saw no change in the level of Futsch-labeled microtubules compared with controls (Fig. 8, compare *C3*, *A3*). Kat-60L1 and Spastin thus regulate the microtubule architecture and promote the complex arborization of larval class IV dendrites through distinct mechanisms.

Discussion

We have shown here a somatodendritic-specific requirement for the microtubule-severing protein Kat-60L1 in the establishment of the full morphology and nociceptive functions of larval class IV

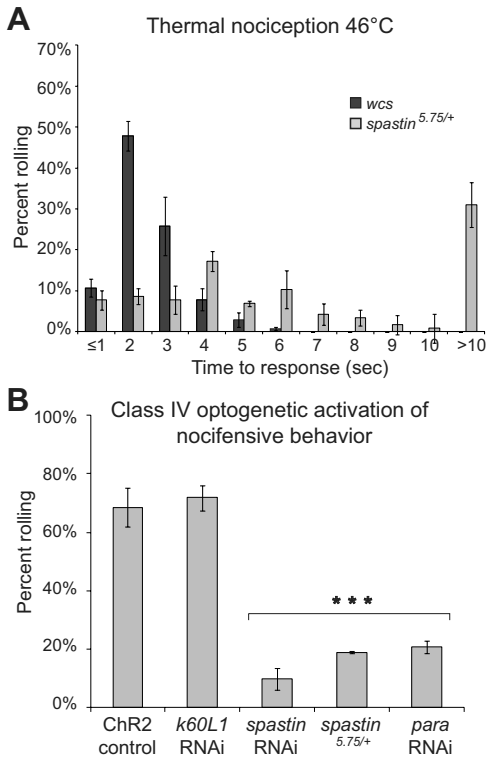

Figure 7. *spastin* mutations reduce NEL but have distinct subcellular consequences compared with *kat-60L1*. ***A***, Similar to *kat-60L1*, *spastin*$^{5.75/+}$-mutant larvae require significantly longer to react in response to a 46°C thermal probe compared with controls ($p < 1 \times 10^{-4}$). ***B***, RNAi knockdown of *kat-60L1* does not impair blue-light ChR2-triggered activation of nociception behavior, which was seen in 72% of larvae versus 69% of controls (control genotype *ppk1.9-GAL4, UAS-ChR2::eYFP/+; UAS-Dicer-2/+*; $p > 0.6$). In contrast, knockdown of either *spastin* or *para* dramatically reduces the response to blue-light stimulation ($p < 1 \times 10^{-4}$).

da neurons. Loss of Kat-60L1 results in fewer and shorter dendrite branches, reducing the density of the arbor spanning the overlying epidermis. This reduced coverage is accompanied by decreased class IV-mediated NEL responses. Optogenetic stimulation bypasses the NEL defect, indicating that Kat-60L1 activity is required only for steps upstream of general excitability and presynaptic function, in the transduction of sensory input mediated by the dendrites and cell body.

Kat-60L1 functions late in dendritic arbor development

The larval md neurons exhibit two stages of arborization: an early, isometric growth phase that establishes dendritic tiling by ~48 h AEL, and a second, scaling growth phase, during which the dendritic arbor expands proportionately with continuing larval growth (Parrish et al., 2009). We observe differences in the density of dendritic coverage only in second and more significantly in late third instars, at 48 and 120 h AEL, respectively. These are not accompanied by obvious defects in tiling. Although mutant 48 h larvae exhibit a slight reduction in arbor density, the role of Kat-60L1 during this time is not essential because, by 72 h AEL, mutant and control arbors are indistinguishable. Only at the late third-instar larval stage (120 h AEL) is the effect of Kat-60L1 loss on arbor density profound. Terminal branches, which are highly dynamic in both genotypes just slightly earlier in development, stabilize by this stage in wild-type, but not mutant, larvae. Kat-60L1 thus plays a central role in the stabilization of terminal class IV dendrite branches, a process that occurs between early and late third-instar larval stages to establish the full class IV arbor. The specific temporal requirement for Kat-60L1 late in larval development provides direct evidence that establishment of the dendritic arbor requires distinct molecules at different times. Even within the phase of scaling growth (48–120 h AEL) the regulation of dendritic branching differs, requiring Kat-60L1 only after 72 h AEL.

Mechanism of Kat-60L1 effects

What is the cell biological mechanism by which Kat-60L1 promotes dendrite outgrowth and stability? To date, no published account demonstrates that Kat-60L1 severs purified microtubules, and exogenous overexpression in *Drosophila* eye or muscle fails to elicit detectable effects on tissue integrity or microtubule distribution (data not shown). This is in stark contrast to the microtubule-severing proteins Spastin and Kat60, both of which induce dramatic breakdown of purified microtubules *in vitro*, and affect microtubule integrity *in vivo*. Nevertheless, we favor a role for Kat-60L1 in microtubule severing based on the following observations. First, the 67% amino acid sequence conservation between the catalytic domains of Kat-60L1 and Kat60 is considerably greater than that between Kat60 and Spastin (44%), consistent with Kat-60L1 sharing a common enzymatic function with these two proteins. Second, data from the Sharp laboratory support a role for Kat-60L1 in severing and depolymerizing microtubule ends, much as they have shown for Kat60 *in vitro* (D.J. Sharp, personal communication; Zhang et al., 2011). Finally, our EB1 analysis revealed reduced numbers of growing microtubules in *kat-60L1*-mutant dendrite branches proximal to the terminal branches. This phenotype is reminiscent of the net microtubule loss observed in both neuromuscular junction boutons and class IV dendrites of *spastin* mutants (Sherwood et al., 2004; Jinushi-Nakao et al., 2007). Together, these results support a model analogous to that proposed for Spastin, in which Kat-60L1 severs microtubules to generate new microtubule fragments from which additional plus-end polymerization occurs, enabling the growth or stabilization of new neurites.

Another possible scenario is suggested by experiments in interphase S2 cells, showing that *Drosophila* Kat60 colocalizes at the cell edge with cortical actin, in an actin-dependent fashion (Zhang et al., 2011). Knockdown of *kat60* by RNAi increases the frequency of actin outgrowth and retraction, as well as the frequency of high-velocity movement in migratory D17 cells. Therefore, like Kat-60L1 in class IV dendrite terminals, Kat60 promotes stability as opposed to motility in these cells. Kat-60L1 could thus be similarly located in the actin cortex of dendrite branches and sever microtubules as they contact the cortex to promote branch stability. Although we rarely observed microtubules in terminal branches, suggesting that these branches are predominantly actin-based, we cannot rule out the limits of our technical ability to visualize EB1 comets in these terminals. Furthermore, because EB1 comets were most clearly visualized in earlier third instar animals, the precise relationship between microtubule polymerization and the acquisition of branch stability remains to be determined. Future experiments that address this and the precise subcellular localization of Kat-60L1, microtubules, and actin across the dendritic arbor will be necessary to distinguish among these mechanisms by which Kat-60L1 promotes branch stability.

Roles of the microtubule-severing proteins in class IV neuron development

Our discovery of a role for Kat-60L1 in larval class IV dendrite arborization, together with earlier studies demonstrating a role for Spastin in these cells (Jinushi-Nakao et al., 2007; Ye et al., 2011), indicates a requirement for not one, but two microtubule-severing

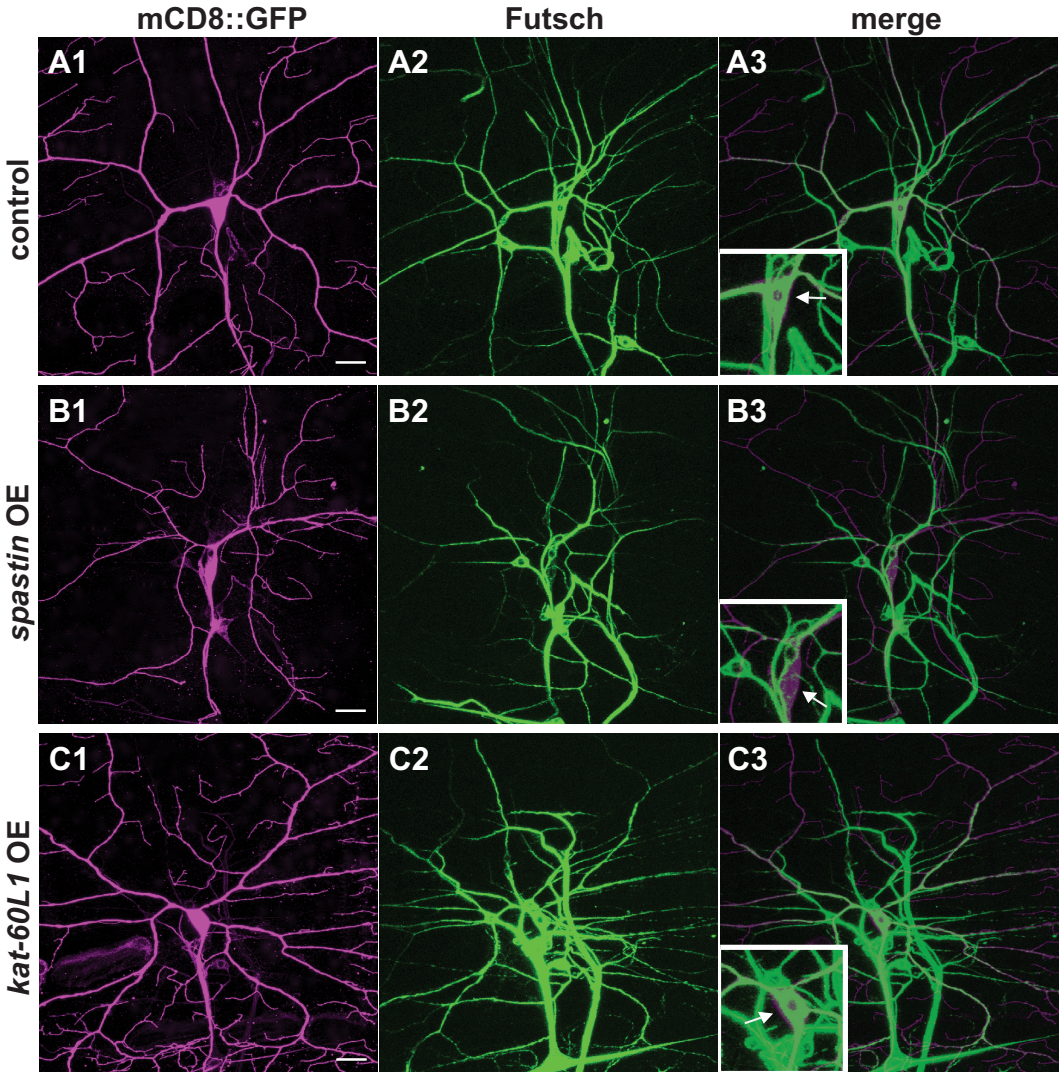

Figure 8. Kat-60L1 and Spastin regulate distinct microtubule populations in the class IV dendritic arbor. ***A–C***, Comparison of Futsch-positive microtubules in class IV ddaC neurons from larvae expressing wild-type (***A1–A3***) or ectopic levels of *spastin* (***B1–B3***) or *kat-60L1* (***C1–C3***). ***A1–C1***, Representative class IV arbors from each genotype expressing *ppk1.9-Gal4, UAS-mCD8::GFP* (GFP staining in magenta). Arbors expressing high levels of *spastin* are strongly reduced in branch complexity (compare ***B1***, ***A1***). ***A2–C2***, Futsch-positive neuronal microtubules are reduced in arbors expressing high levels of *spastin* compared with wild-type or ectopic *kat-60L1* expression (compare ***B2***, ***A2***, ***C2***). ***A3–C3***, Merged images reveal that the class IV cell body (arrow, insets) and proximal branches in control and *kat-60L1*-overexpressing cells are rich in Futsch-positive microtubules, in contrast to *spastin*-overexpressing neurons. Scale bars, 20 μm.

proteins in this process. Although loss of Spastin and Kat-60L1 both reduce the dendritic arbor and NEL behavior in these cells, they have independent roles in the class IV neurons. In contrast to *kat-60L1* mutations, *spastin* mutations affect both axon and dendrite morphology (Ye et al., 2011), and the inability of optogenetic stimulation to bypass the reduced NEL phenotype indicates that axonal function is also compromised. Additionally, these morphological and behavioral defects do not arise from a reduction in distal growing microtubules, as EB1 dynamics in *spastin* mutants are unaffected. Instead, stable, Futsch-positive microtubules are sensitive to Spastin overexpression, and resistant to Kat-60L1 activity. While we do not yet understand how Spastin loss compromises the dendritic arbor, it almost certainly does so through a mechanism distinct from Kat-60L1 and, indeed, may even be an indirect consequence of its effects on axon development.

The microtubule-generating function for Kat-60L1 in larval class IV dendrites suggested by our data also reveals that Kat-60L1 plays strikingly distinct roles at two different stages of development within the same cells. In the larval stage, Kat-60L1 promotes net microtubule gain and class IV dendritic outgrowth, but in the pupal stage it has an opposite function, promoting net microtubule loss during class IV dendritic pruning (Lee et al., 2009). Such differences may arise from the regulation of Kat-60L1 itself, which remains to be understood. Differences between microtubules and their associated proteins at each developmental stage may also dictate the specific consequence of Kat-60L1 enzymatic activity. The microtubule-associated protein (MAP) Tau is thought to regulate the susceptibility of microtubules to severing by Kat60 (Qiang et al., 2006; Yu et al., 2008), while Spastin is reported to target stable microtubule populations (Jinushi-Nakao et al., 2007). Other MAPs, or post-translational modifications of microtubules, may serve to differentiate microtubule susceptibility to net polymerization or depolymerization following Kat-60L1 activity. A reasonable prediction would be that compared with larval dendrites, pupal dendrites are rich in microtubules susceptible to Kat-60L1 severing, and lacking in molecules required for microtubule fragment stabilization and subsequent polymerization.

The identification of Kat-60L1 as a late-stage, compartment-specific regulator of dendrite arbor growth adds to our understanding of the diverse ways in which this family of microtubule-severing proteins is deployed. The differential consequences of *kat-60L1* expression at different stages, as well as the additional requirement for Spastin in these neurons, provide further evidence that this protein family evolved to allow for unique and precise regulation of the neuronal cytoskeleton in multiple developmental contexts.

Kat-60L1 loss induces relatively moderate changes in the larval dendrite arbor (~20% decreases in the area covered by dendrites, the numbers of terminal dendrites, or terminal dendrite lengths), and reduces the nocifensive responses mediated by these neurons by nearly half. This suggests that the full NEL behavior requires complete dendritic arborization, particularly of terminal branch outgrowth. This could reflect a simple spatial requirement, in that full branch density is needed to effectively transduce nocifensive stimuli. However, it also suggests the possibility of a unique role for the terminal dendrite branches in class IV nociceptive functioning. Kat-60L1 upregulation of microtubule polymerization, for example, could not only stabilize terminal processes but also enable delivery of or scaffolding for receptors or other machinery critical to sensory function in these branches.

Our data support the idea that dendrite arborization is regulated by distinct molecules at distinct developmental time points, rather than through the repetition of a single "branching program." Differential combinations of these regulatory pathways, including the activity of microtubule-severing proteins, contribute to establishment of the unique form and functions of the class IV multidendritic neurons.

References

Ainsley JA, Pettus JM, Bosenko D, Gerstein CE, Zinkevich N, Anderson MG, Adams CM, Welsh MJ, Johnson WA (2003) Enhanced locomotion caused by loss of the Drosophila DEG/ENaC protein Pickpocket1. Curr Biol 13:1557–1563.

Brand AH, Perrimon N (1993) Targeted gene expression as a means of altering cell fates and generating dominant phenotypes. Development 118:401–415.

Caldwell JC, Tracey WD Jr (2010) Alternatives to mammalian pain models 2: using Drosophila to identify novel genes involved in nociception. Methods Mol Biol 617:19–29.

Chintapalli VR, Wang J, Dow JA (2007) Using FlyAtlas to identify better Drosophila melanogaster models of human disease. Nat Genet 39:715–720.

Dietzl G, Chen D, Schnorrer F, Su KC, Barinova Y, Fellner M, Gasser B, Kinsey K, Oppel S, Scheiblauer S, Couto A, Marra V, Keleman K, Dickson BJ (2007) A genome-wide transgenic RNAi library for conditional gene inactivation in Drosophila. Nature 448:151–156.

Franke JD, Montague RA, Kiehart DP (2010) Nonmuscle myosin II is required for cell proliferation, cell sheet adhesion and wing hair morphology during wing morphogenesis. Dev Biol 345:117–132.

Grueber WB, Jan LY, Jan YN (2002) Tiling of the Drosophila epidermis by multidendritic sensory neurons. Development 129:2867–2878.

Grueber WB, Ye B, Yang CH, Younger S, Borden K, Jan LY, Jan YN (2007) Projections of Drosophila multidendritic neurons in the central nervous system: links with peripheral dendrite morphology. Development 134:55–64.

Honjo K, Hwang RY, Tracey WD (2012) Optogenetic manipulation of neural circuits and behavior in *Drosophila* larvae. Nature Protocols 7:1470–1478.

Hughes CL, Thomas JB (2007) A sensory feedback circuit coordinates muscle activity in Drosophila. Mol Cell Neurosci 35:383–396.

Hwang RY, Zhong L, Xu Y, Johnson T, Zhang F, Deisseroth K, Tracey WD (2007) Nociceptive neurons protect Drosophila larvae from parasitoid wasps. Curr Biol 17:2105–2116.

Jinushi-Nakao S, Arvind R, Amikura R, Kinameri E, Liu AW, Moore AW (2007) Knot/Collier and cut control different aspects of dendrite cytoskeleton and synergize to define final arbor shape. Neuron 56:963–978.

Lee HH, Jan LY, Jan YN (2009) Drosophila IKK-related kinase Ik2 and Katanin p60-like 1 regulate dendrite pruning of sensory neuron during metamorphosis. Proc Natl Acad Sci U S A 106:6363–6368.

Mattie FJ, Stackpole MM, Stone MC, Clippard JR, Rudnick DA, Qiu Y, Tao J, Allender DL, Parmar M, Rolls MM (2010) Directed microtubule growth, +TIPs, and kinesin-2 are required for uniform microtubule polarity in dendrites. Curr Biol 20:2169–2177.

McNally FJ, Vale RD (1993) Identification of katanin, an ATPase that severs and disassembles stable microtubules. Cell 75:419–429.

Meijering E, Jacob M, Sarria JC, Steiner P, Hirling H, Unser M (2004) Design and validation of a tool for neurite tracing and analysis in fluorescence microscopy images. Cytometry A 58:167–176.

Moore AW (2008) Intrinsic mechanisms to define neuron class-specific dendrite arbor morphology. Cell Adh Migr 2:81–82.

Parrish JZ, Xu P, Kim CC, Jan LY, Jan YN (2009) The microRNA bantam functions in epithelial cells to regulate scaling growth of dendrite arbors in drosophila sensory neurons. Neuron 63:788–802.

Qiang L, Yu W, Andreadis A, Luo M, Baas PW (2006) Tau protects microtubules in the axon from severing by katanin. J Neurosci 26:3120–3129.

Roll-Mecak A, McNally FJ (2010) Microtubule-severing enzymes. Curr Opin Cell Biol 22:96–103.

Roll-Mecak A, Vale RD (2008) Structural basis of microtubule severing by the hereditary spastic paraplegia protein spastin. Nature 451:363–367.

Sharp DJ, Ross JL (2012) Microtubule-severing enzymes at the cutting edge. J Cell Sci. Advance online publication. Retrieved May 17, 2012. PMID: 22595526.

Sherwood NT, Sun Q, Xue M, Zhang B, Zinn K (2004) Drosophila spastin regulates synaptic microtubule networks and is required for normal motor function. PLoS Biol 2:e429.

Siddiqi O, Benzer S (1976) Neurophysiological defects in temperature-sensitive paralytic mutants of Drosophila melanogaster. Proc Natl Acad Sci U S A 73:3253–3257.

Stone MC, Roegiers F, Rolls MM (2008) Microtubules have opposite orientation in axons and dendrites of Drosophila neurons. Mol Biol Cell 19:4122–4129.

Thibault ST, Singer MA, Miyazaki WY, Milash B, Dompe NA, Singh CM, Buchholz R, Demsky M, Fawcett R, Francis-Lang HL, Ryner L, Cheung LM, Chong A, Erickson C, Fisher WW, Greer K, Hartouni SR, Howie E, Jakkula L, Joo D,et al. (2004) A complementary transposon tool kit for Drosophila melanogaster using P and piggyBac. Nat Genet 36:283–287.

Tomancak P, Beaton A, Weiszmann R, Kwan E, Shu S, Lewis SE, Richards S, Ashburner M, Hartenstein V, Celniker SE, Rubin GM (2002) Systematic determination of patterns of gene expression during Drosophila embryogenesis. Genome Biol 3:RESEARCH0088.

Tracey WD Jr, Wilson RI, Laurent G, Benzer S (2003) painless, a Drosophila gene essential for nociception. Cell 113:261–273.

Williams DW, Kondo S, Krzyzanowska A, Hiromi Y, Truman JW (2006) Local caspase activity directs engulfment of dendrites during pruning. Nat Neurosci 9:1234–1236.

Wu CF, Ganetzky B (1980) Genetic alteration of nerve membrane excitability in temperature-sensitive paralytic mutants of Drosophila melanogaster. Nature 286:814–816.

Ye B, Kim JH, Yang L, McLachlan I, Younger S, Jan LY, Jan YN (2011) Differential regulation of dendritic and axonal development by the novel kruppel-like factor dar1. J Neurosci 31:3309–3319.

Yu W, Qiang L, Solowska JM, Karabay A, Korulu S, Baas PW (2008) The microtubule-severing proteins spastin and katanin participate differently in the formation of axonal branches. Mol Biol Cell 19:1485–1498.

Zanic M, Stear JH, Hyman AA, Howard J (2009) EB1 recognizes the nucleotide state of tubulin in the microtubule lattice. PLoS One 4:e7585.

Zhang D, Rogers GC, Buster DW, Sharp DJ (2007) Three microtubule severing enzymes contribute to the "Pacman-flux" machinery that moves chromosomes. J Cell Biol 177:231–242.

Zhang D, Grode KD, Stewman SF, Diaz-Valencia JD, Liebling E, Rath U, Riera T, Currie JD, Buster DW, Asenjo AB, Sosa HJ, Ross JL, Ma A, Rogers SL, Sharp DJ (2011) Drosophila katanin is a microtubule depolymerase that regulates cortical-microtubule plus-end interactions and cell migration. Nat Cell Biol 13:361–370.

Zhong L, Hwang RY, Tracey WD (2010) Pickpocket is a DEG/ENaC protein required for mechanical nociception in *Drosophila* larvae. Curr Biol 20:429–434.

Zhong L, Bellemer A, Yan H, Honjo K, Robertson J, Hwang RY, Pitt GS, Tracey WD (2012) Thermosensory and non-thermosensory isoforms of *Drosophila melanogaster* TRPA1 reveal heat sensor domains of a thermoTRP channel. Cell Rep 1:43–55.